Available online at www.sciencedirect.com
SCIENCE DIRECT®
Journal of Petroleum Science and Engineering 41 (2004) 253–267
JOURNAL OF PETROLEUM SCIENCE & ENGINEERING
www.elsevier.com/locate/petrol

Fluid flow in gas condensate reservoirs: the interplay of forces and their relative strengths

Jann-Rune Ursin*

Stavanger University College, Department of Petroleum Engineering, PO Box 8002, Stavanger, 4068, Norway

Accepted 12 September 2003

Abstract

Natural production from gas condensate reservoirs is characterized by gas condensation and liquid dropout in the reservoir, first in the near wellbore volume, then as a cylindrical shaped region, dynamically developing into the reservoir volume. The effects of liquid condensation are reduced productivity and loss of production. Successful forecast of well productivity and reservoir production depends on detailed understanding of the effect of various forces acting on fluid flow in time and space. The production form gas condensate reservoirs is thus indirectly related to the interplay of fundamental forces, such as the viscosity, the capillary, the gravitational and the inertial force and their relative strengths, demonstrated by various dimensionless numbers.

Dimensionless numbers are defined and calculated for all pressure and space coordinates in a test reservoir. Various regions are identified where certain forces are more important than others. Based on reservoir pressure development, liquid condensation and the numerical representation of dimensionless numbers, a conceptual understanding of a varying reservoir permeability has been reached.

The material balance, the reservoir fluid flow and the wellbore flow calculations are performed on a cylindrical reservoir model. The ratios between fundamental forces are calculated and dimensionless numbers defined. The interplay of forces, demonstrated by these numbers, are calculated as function of radial dimension and reservoir pressure.

Keywords: Gas condensate; Fluid flow; Dimensionless numbers; Condensate saturation; Effective permeability

1. Introduction

Gas condensate reservoirs are characterized by gas condensation and liquid drop out in the reservoir under normal production. The extent of condensation under isothermal depletion varies considerably and is to a large extent related to the temperature difference between the critical temperature of the fluid and the reservoir temperature. In gas condensate reservoirs where these temperatures are naturally close, relatively large amount of liquid condensate can drop out, causing alternating flow behavior on several scales in the reservoir (Williams and Dawe, 1989).

The drop out of liquids represents to a large extent lost production and the condensate deposited is generally considered to be a hindrance to normal gas flow. In particular is a problem in the near well region, where loss of well productivity is a persistent prob-

* Fax: +47-5183-1050.
E-mail address: jann-rune.ursin@tn.his.no (J.-R. Ursin).

0920-4105/$ - see front matter © 2003 Elsevier B.V. All rights reserved.
doi:10.1016/j.profnurs.2003.09.005

lem. The general concern and uncertainty related to well deliverability (Fevang and Whitson, 1996) and to reservoir productivity in general are basically a result of the continued liquid drop out in gas condensate reservoirs.

Reservoir modelling and numerical simulation of gas and gas condensate production depend clearly on accurate descriptions of both fluid(s) and reservoir formations. In addition, proper understanding of fundamental aspects of the dynamics of gas and liquid condensate during production is certainly not to be underestimated. The basic understanding of fundamental forces and their relative strengths can be directly related to the effective permeability (Raghavan and Jones, 1996; Fulcher et al., 1983; Morrow and Songkran, 1981).

In this article, we will discuss the various fundamental forces, their relative strengths and the variation in strengths as function of time and space. The purpose of this article is to present a principle set of forces, the set of ratios between forces and on this basis, define a complete set of dimensionless numbers. These numbers are presented as function of pressure and radius position in a cylindrical test model, simulating somewhat idealized reservoir conditions.

2. Fundamental forces

At pressures lower than the dewpoint pressure ($p < p_{dew}$), two hydrocarbon phases will be present in the reservoir. During the process of natural gas production, four fundamental forces will act on the fluids. These forces are the viscosity (V), the capillary (C), the gravitational (G) and the inertial (I) force.

The viscous forces is commonly understood as the intermolecular interaction within the fluid itself and relative to the bounding conditions such as the pore channel wall or other fluids. This force causes a velocity profile to develop across the flow channel and is responsible for the viscous pressure loss in the reservoir.

In the presence of two or more phases, i.e., gas and liquid condensate, the interface between the two phases represents a pressure difference under dynamical flow conditions. The importance of capillary forces is related to wettability in general and the spreading of the wetting phase in particular (Coskuner, 1999).

The gravitational force is always active in all parts of the reservoir. In reservoir fluid flow, the gravity force can be of importance in situations where the fluids have different densities, as in the case of gas and liquid condensate.

The inertial force is associated with the redirection of fluid flow in the porous media. In linear flow, i.e., flow in a strait tube, no inertial forces are active. In a porous media, on the other hand, a continuous redirection of flow is taking place as the hydrocarbon molecules are moving between the grain minerals.

2.1. Ratio of viscous and capillary forces

The ratio of viscous and capillary forces is easily illustrated by an example of linear flow in a cylindrical pore channel of length L and diameter $2R$, as depicted in Fig. 1. The liquid condensate is believed

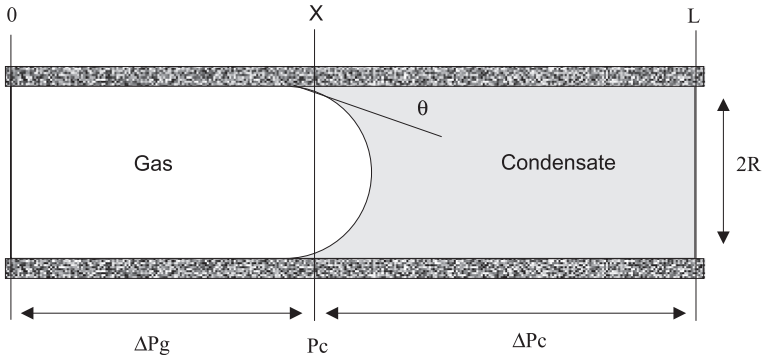

Fig. 1. Cylindrical pore channel for viscous and capillary pressure drop.

to wet the solid surface of the pore channel, and the wetting angle is θ. The flow of gas and condensate is taking place at a constant pore velocity v_g.

The viscous pressure loss ΔP_V, is the sum of the pressure loss in the gas, ΔP_g and in the condensate phase, ΔP_o. Using the Poiseuille's law, we may write

$$\Delta P_V = \Delta P_g + \Delta P_o = 8\frac{v_g}{R^2}(\mu_g x + \mu_o(L-x)) \quad (1)$$

where μ_g and μ_o are the viscosity of gas and condensate, respectively. x is the position of the capillary interface and is on average equal to $L/2$.

The capillary pressure drop P_C, across the interface in a capillary tube is given as

$$P_C = \frac{2\sigma_{go}\cos(\theta)}{R} \quad (2)$$

where σ_{go} is the interfacial tension and θ is the wetting angle.

The ratio between viscous and capillary forces is therefore written

$$\frac{\Delta P_V}{P_C} = \frac{v_g\mu_o}{\sigma_{go}\cos(\theta)}\frac{2L}{R}\left(\frac{\mu_g}{\mu_o}+1\right) \quad (3)$$

We may safely assume the gas viscosity to always be less than the condensate viscosity, i.e., $\mu_g \ll \mu_o$. For a capillary tube, the ratio of tube length over tube radius would normally be much larger than one, while this ratio in an interconnecting pore network could be assumed to be close to one, i.e., $2L/R \sim 1$.

Based on these assumptions, a capillary number N_C which demonstrates the ratio of viscous over capillary forces can be defined,

$$N_C = \frac{v_g\mu_o}{\sigma_{go}\cos(\theta)} \quad (4)$$

2.2. Ratio of gravitational and capillary forces

The condensation of gas leads to the formation of liquid condensate which has a higher density than the gas phase, where $\rho_o > \rho_g$ for all pressures lower than the dew point pressure, $p < p_{dew}$.

The gravitational force will act on a freely floating liquid condensate drop, by pulling it downwards towards the lower edge of the pore channel, as depicted in Fig. 2. Similarly, we may also assume the gravitational force to be responsible for the slow and constant movement of liquid condensate to lower potential energy, as small droplets on the pore walls itself.

Assuming the liquid drop to be small, we may consider the droplet to be spherical, with a radius R_d. The gravitational pressure difference or buoyancy, ΔP_G, forcing the droplet on a downward curving path is

$$\Delta P_G = \frac{R_d}{3}\Delta\rho_{go}g, \quad (5)$$

where $\Delta\rho_{go} = \rho_o - \rho_g$ is the density difference and g is the gravitational constant.

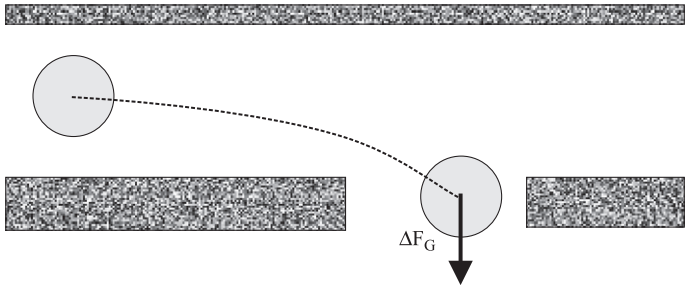

Fig. 2. Linear pore channel for gravitational effect.

The ratio of the gravitational force over the capillary force is thus

$$\frac{\Delta P_G}{P_C} = \frac{R_d R}{3} \frac{\Delta \rho_{go} g}{\sigma_{go} \cos(\theta)} \tag{6}$$

If we associate the surface $R_d R/3$ with an imaginable surface characterized by the absolute permeability k, of the porous medium, the ratio between the gravitational force and the capillary force can be expressed by the Bond number

$$N_B = \frac{k \Delta \rho_{go} g}{\sigma_{go} \cos(\theta)} \tag{7}$$

2.3. Ratio of viscous and gravitational forces

A dimensionless number describing the ratio of viscous over gravitational forces is easily defined as the ratio of the capillary number over the Bond number, $N(V/G) = N_C/N_B$, and we find

$$N(V/G) = \frac{\upsilon_g \mu_o}{k \Delta \rho_{go} g} \tag{8}$$

2.4. Ratio of inertial and viscous forces

Inertial forces are present in all aspects of fluid flow in porous media. The inertial force is responsible for keeping the fluid molecules on the track when moving around the grain minerals. In a curved pore channel as depicted in Fig. 3, the inertial force will insure the nonlinear movement of fluid molecules around the two circular grains.

The force acting on gas molecules following a circular path of radius R_r can be written

$$\Delta F_I = A \Delta L \rho_g \frac{\upsilon_g^2}{R_r}, \tag{9}$$

where A is the cross-section of the pore channel, ΔL is a line segment along the flow path and υ_g is the average gas velocity.

Using Poiseuille's equation for fluid flow in a cylindrical tube with a constant cross-section $A = \pi R^2$, as presented above, the pressure drop per length is

$$\frac{\Delta P_I}{\Delta L} = \rho_g \frac{\upsilon_g^2}{R_r}. \tag{10}$$

Similarly, we may define the viscous pressure drop per length for viscous flow by using Poiseuille's equation, and by comparing the two expressions, we find the ratio,

$$\frac{\Delta P_V / \Delta L}{\Delta P_I / \Delta L} = \frac{\mu_g}{\upsilon_g \rho_g} \frac{8 R_r}{R^2}, \tag{11}$$

where υ_g, ρ_g and μ_g are the gas velocity, density and viscosity, respectively, of the flowing gas.

Considering the length $8R_r/R^2$ to be proportional to the square root of the permeability k, we can define a dimensionless number demonstrating the ratio between viscous and inertial forces

$$N(V/I) = \frac{\mu_g}{v_g \rho_g \sqrt{k}} \tag{12}$$

The dimensionless number $N(V/I)$ is related to porous flow, but can be associated with the reciprocal

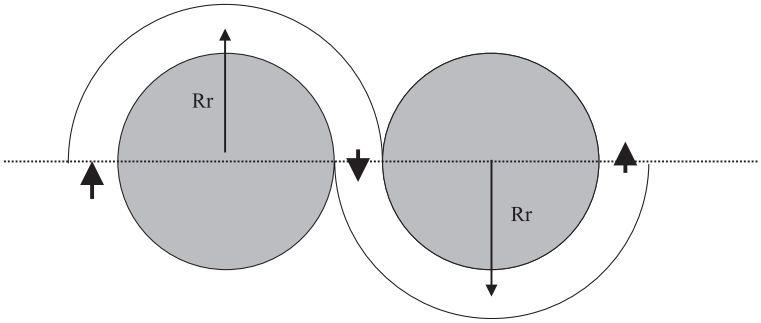

Fig. 3. Circular curved pore channel depicting inertial forces.

of Reynolds number, as generally the same variables are involved.

2.5. Definition of dimensionless numbers

As seen above, four dimensionless numbers can be defined as ratios of viscous, capillary, gravitational and inertial forces; $N(C/V)=1/N_C$, $N(C/G)=1/N_B$, $N(V/G)=N_C/N_B$ and $N(V/I)$ as above.

Based on the four fundamental forces, there exist all together 12 dimensionless ratios of which six are the reciprocal of the others. These ratios can be systematically presented in the form of a matrix:

Forces	C	V	G	I
C	1	$N(C/V)$	$N(C/G)$	$N(C/I)$
V	$N(V/C)$	1	$N(V/G)$	$N(V/I)$
G	$N(G/C)$	$N(G/V)$	1	$N(G/I)$
I	$N(I/C)$	$N(I/V)$	$N(I/G)$	1

It is practical to view the dimensionless numbers in the matrix above in relation to the relative strength of the forces involved. Since the capillary force, in a strongly wetted porous medium, can be considered to be the strongest force, followed by the viscous and then the gravitational and the inertial forces as the weakest forces, we may choose to compare the different forces by viewing the following dimensionless numbers: $N(C/V)$, $N(C/G)$, $N(C/I)$, $N(V/G)$, $N(V/I)$ and $N(G/I)$ (see the dimensionless number above the diagonal in the matrix above).

Following the listing above: $N(C/V)$, $N(C/G)$, $N(V/G)$ and $N(I/V)$ are already known. The numbers $N(I/C)$ and $N(I/G)$ are unknown, but can easily be defined.

$$N(I/C)=N(I/V)/N(C/V) \tag{13}$$

$$N(I/G)=N(I/V)/N(V/G) \tag{14}$$

Finally, the following six dimensionless numbers can be defined:

$$N(C/V)=\frac{\sigma_{go}\cos(\theta)}{\upsilon_g\mu_o}, \tag{15}$$

$$N(C/G)=\frac{\sigma_{go}\cos(\theta)}{k\Delta\rho_{go}g}, \tag{16}$$

$$N(V/G)=\frac{\upsilon_g\mu_o}{k\Delta\rho_{go}g}, \tag{17}$$

$$N(C/I)=\frac{\mu_g}{\mu_o}\frac{\sigma_{go}\cos(\theta)}{\upsilon_g^2\rho_g\sqrt{k}}, \tag{18}$$

$$N(V/I)=\frac{\mu_g}{\upsilon_g\rho_g\sqrt{k}}, \tag{19}$$

$$N(G/I)=\frac{\mu_g}{\mu_o}\frac{g\Delta\rho_{go}\sqrt{k}}{\upsilon_g^2\rho_g}. \tag{20}$$

3. Calculation of dimensionless numbers

The parameters used in the definition of dimensionless numbers, Eqs. (15)–(20), are limited to the following seven independent variables: υ_g, μ_o, μ_g, σ_{go}, ρ_g, ρ_o and k. The wetting angle θ is assumed to be close to zero, indicating strongly oil wet conditions. A representation of the dimensionless numbers are given by a numerical representation of these variables, where a test case scenario, involving data from an actual light gas condensate reservoir has been chosen.

3.1. PVT simulations

The molar composition of the test fluid is given in Table 1. The corresponding reservoir pressure and temperature are 437 bar and 392 K, respectively.

PVT simulations, based on the data presented above, have been performed using a commercial available PVT simulator (PVTsim from Calsep), where the Soave-Redlich-Kwong (SRK) equation of state with the Peneloux molar volume correction is used. The results of these simulations are presented in Fig. 4 for the viscosity data, where the calculations are based on the corresponding states principles in the form suggested by Pedersen et al. (1984) and Pedersen

Table 1
Molar composition (in %) of gas condensate test fluid

Compounds	N_2	CO_2	C_1	C_2	C_3	iC_4	nC_4	iC_5	nC_5	C_6	C_7	C_8	C_9	C_{10}^+
Composition	0.78	8.72	71.00	8.56	4.67	0.71	1.23	0.41	0.41	0.45	0.66	0.70	0.41	1.29

and Fredenslund, (1987). Fig. 5 presents the interfacial tension data, calculated using the procedure of Weinaug and Katz (1943), where the interfacial tension is expressed in terms of the parachors of the individual components. In Fig. 6 for the density data. All variables, μ_o, μ_g, σ_{go}, ρ_o, ρ_g and $\Delta\rho_{go}$ are given as function of pressure, ranging from 0 to 450 bar for gas variables and from 0 to 367 bar (dew point pressure) for those variables describing liquid condensate behavior.

3.2. Reservoir simulations

In order to calculate the gas velocity v_g, under reservoir conditions, simulation of gas flow has to be performed. A custom-made reservoir simulation model has been used in these simulations, where idealized reservoir conditions have been assumed.

The reservoir is cylindrical shaped with the well at the center position. The outer radius $r_w = 360$ m and the well radius $r_w = 0.175$ m. The thickness of the reservoir, $h = 50$ m and the well is perforated along the whole reservoir thickness. Porosity and connate water saturation are both 20%. The reservoir is homogenous with an isotropically distributed absolute permeability k equal to 10 mD. The pore volume V_p of approximately 4 10^6 Sm^3 is produced at a constant surface flow rate, $q_g = 0.5$ 10^6 Sm^3/day.

The pressure profiles given in Fig. 7, represents the mean reservoir pressure $\bar{p}$ and the bottom hole pressure p_{bh}. As seen from this figure, the production period down to a minimum bottom hole pressure of 10 bar is approximately 3.5 years.

The reservoir pressure distribution in time and space can be represented by the following simple formula, insuring a radially and logarithmic increasing pressure distribution under semi steady-state flow conditions

$$p(r,t) = p_{bh}(t) + (\bar{p}(t) - p_{bh}(t))\frac{\ln(r/r_w)}{\ln(r_e/r_w)} \qquad (21)$$

Fig. 8 shows the pressure field as function of time and radius position. The well skin is neglected ($S = 0$) in the calculation above and similarly is the increased pressure drop induced by liquid condensation in the reservoir not considered at this point. The numerical representation of the pressure field shows that after a certain time, the pressure in most parts of the reservoir is lower than the dew point pressure and that this situation prevails for about 3/4 of the total production

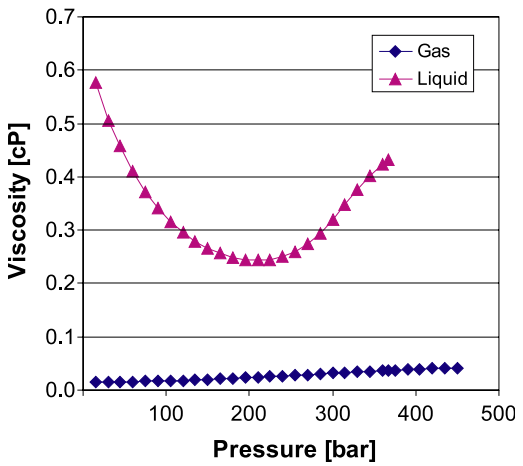

Fig. 4. Gas and condensate viscosity as function of pressure.

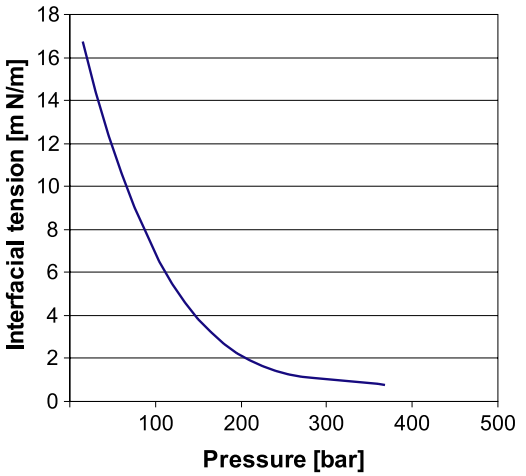

Fig. 5. Interfacial tension as function of pressure.

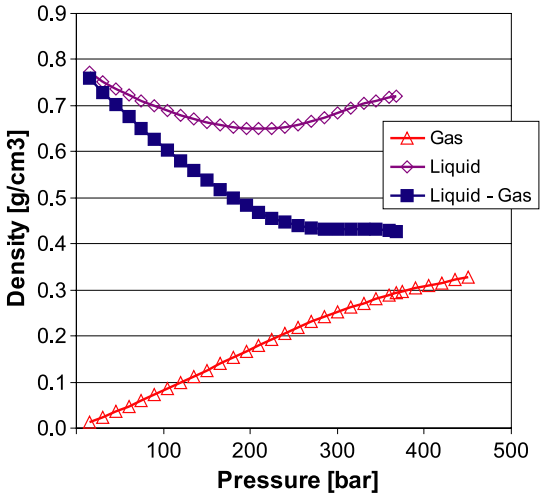

Fig. 6. Gas and condensate density as function of pressure.

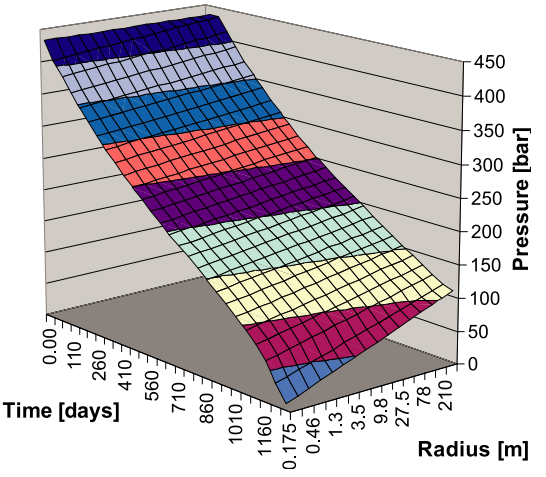

Fig. 8. The pressure distribution in time and space for a cylindrical reservoir.

period. Thus, the process of liquid drop out is active in most parts of the reservoir for most of the production period.

3.3. Pore velocity

The surface gas rate $q_{g,sc}$ is constant as pointed out above. Thus, the reservoir gas rate $q_{g,res}$ is given

$$q_{g,res}(p) = B_g(p) \cdot q_{g,sc}, \tag{22}$$

where B_g is the volume factor for gas at pressure p.

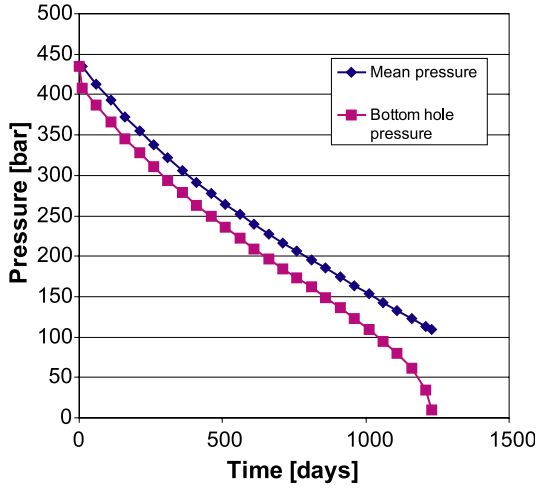

Fig. 7. Pressure decline in cylindrical reservoir as function of time.

The bulk velocity $v_{g,bulk}$ at a radial cross-section $A_{res} = 2\pi r \cdot h$ in the reservoir is thus given

$$v_{g,bulk}(r,p) = \frac{B_g(p) q_{g,sc}}{2\pi r \cdot h}. \tag{23}$$

The pore velocity is proportional to the bulk velocity, $v_{g,pore} = v_{g,bulk}/(\phi(1\text{-}S_{wc})\ \cos^2(\alpha))$, where α is the tortuosity angle, defining the crookedness of porous gas flow. ϕ and S_{wc} are the porosity and connate water saturation, respectively. The gas volume factor B_g is defined by using the extended real gas law where liquid condensation in the reservoir is represented by the surface molar liquid–gas ratio. The gas pore velocity is then written

$$v_{g,pore}(r,p) = \frac{1}{\phi(1-S_{wc})\cos^2(\alpha)} \frac{Z(p)}{2\pi r \cdot h} \frac{T_{res}}{T_{sc}} \times \frac{p_{sc}}{p}(1 + R_{MLG}(p)) \cdot q_{g,sc}, \tag{24}$$

where R_{MLG} is the molar liquid–gas ratio (at surface conditions). The pore velocity, above, is not corrected for the effect of liquid condensation that will reduce the pore space available for gas transport. Thus, the effective pore velocity, in presence of liquid condensate, will always be higher than presented in the formula above.

Fig. 9 shows the pore velocity field in the radius–pressure plane. The lowest flow velocity $v_{g,pore} = 0.1$

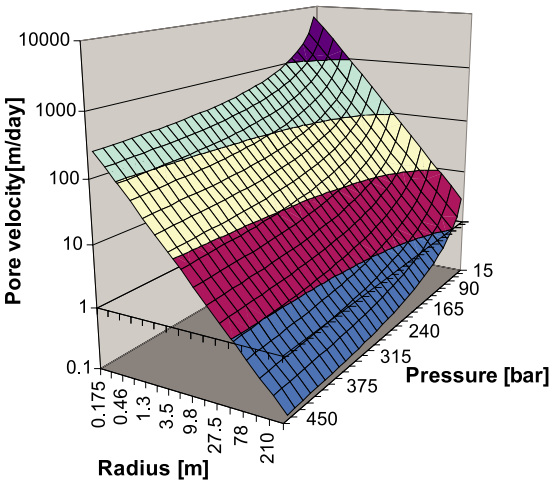

Fig. 9. Pore velocity as function of reservoir radius and pressure.

m/day, is found at the reservoir outer boundary and at initial pressure, while the highest pore velocity is approximately equal to 6500 m/day, close to the well at minimum bottom hole pressure. The pore velocity is increasing as the gas moves closer to the wellbore for all pressures, but the highest pore velocities are found at the lowest reservoir pressures. The increase in pore velocity is increasing as the pressure is decreasing.

3.4. Dimensionless numbers

Based on the calculations performed above, we are now in a position to calculate the dimensionless numbers defined in Eqs. (15)–(20).

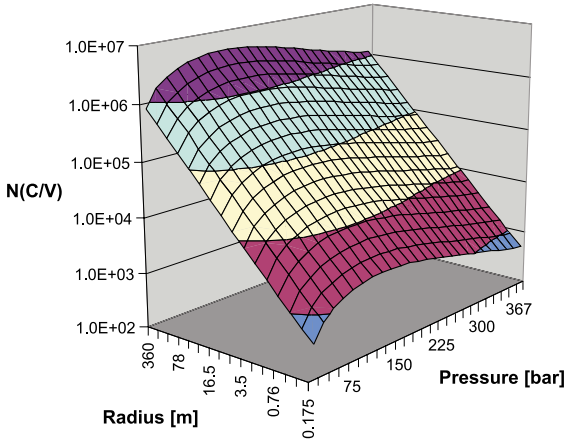

Fig. 10. Normalized ratio of viscous and capillary forces.

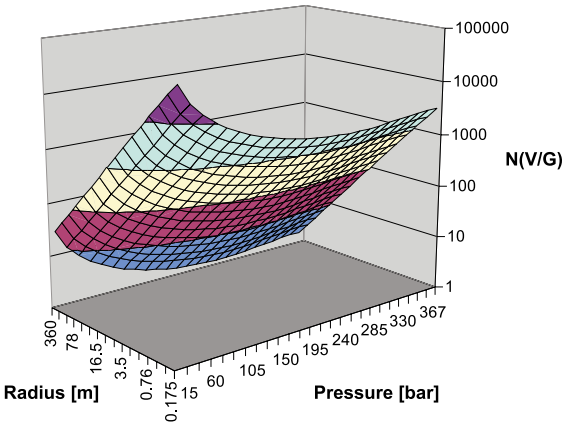

Fig. 11. Normalized ratio of viscous and gravitational forces.

All plots of dimensionless number (Figs. 10, 11, 13, 14 and 15 are given as functions of radial distance and pressure, except the dimensionless number $N(C/G)$, Fig. 12, which does not depend on pore velocity and thus is radial independent. All plots depict the absolute value of ratios between all four forces.

The dynamical range of the various dimensionless numbers as well as the pore velocity are represented by minimum and maximum numbers and presented in Table 2.

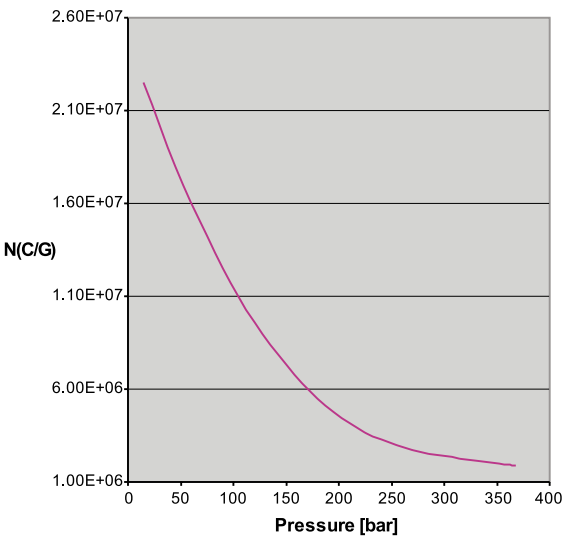

Fig. 12. Normalized ratio of capillary and gravitational forces.

Table 2
Dynamic range of pore velocity and dimensionless numbers

			relative range
1.3×10^{-1}	$\leq v_{g,pore} \leq$	6.4×10^{3}	4.8×10^{4}
3.9×10^{2}	$\leq N(C/V) \leq$	4.6×10^{6}	1.2×10^{4}
1.8×10^{6}	$\leq N(C/G) \leq$	2.3×10^{7}	1.2×10^{1}
2.1×10^{4}	$\leq N(C/I) \leq$	6.9×10^{11}	3.3×10^{7}
1.2×10^{0}	$\leq N(V/G) \leq$	5.7×10^{4}	4.8×10^{4}
5.2×10^{1}	$\leq N(V/I) \leq$	2.6×10^{5}	5.0×10^{3}
9.1×10^{-4}	$\leq N(G/I) \leq$	1.7×10^{5}	1.9×10^{8}

As can be seen from Table 2, the dynamical range of the dimensionless numbers $N(C/V)$, $N(V/G)$ and $N(V/I)$, do all span a range of about four orders of magnitude, where the important parameter is the pore velocity. In the case of the ratio of capillary over gravity forces, $N(C/G)$, there is no pore velocity dependency and the dynamical range is only about one order of one magnitude. For $N(I/C)$ and $N(I/G)$, the dynamical range is in the order of about eight orders of magnitude, proportional to the square of pore velocity.

The absolute scale of dimensionless numbers, as presented in Figs. 10–15, does most likely not describe the competition between the four forces correctly. In Fig. 10, as an example, the capillary force is totally dominating the viscous force at all times, in all parts of the reservoir by at least two orders of magnitude. This is obviously in disagreement with observations and does not represent a correct interpretation of the data presented. On the other hand, it is more conceivable to interpret the observation in Fig. 10, as a statement that the relative importance of the capillary force compared to the viscous force is drastically reduced when approaching the well.

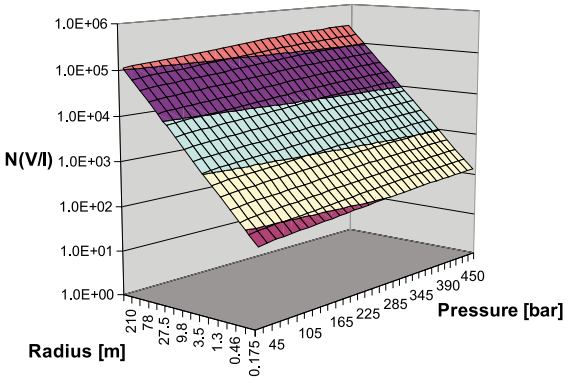

Fig. 13. Normalized ratio of inertial and viscous forces.

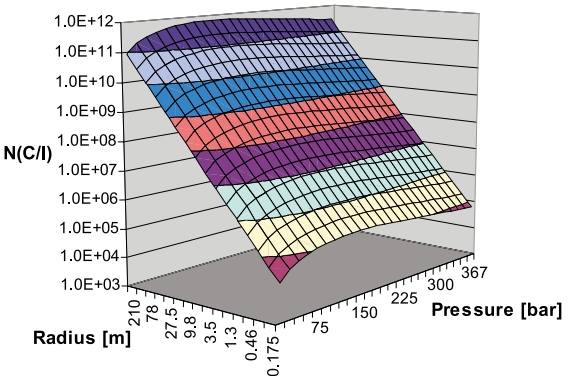

Fig. 14. Normalized ratio of inertial and capillary forces.

Based on the relative change of the different dimensionless numbers, the following general statements can be made:

1. The relative importance of the inertial force compared to the capillary, the gravitational and to a lesser degree the viscous force, is drastically increasing as function of decreasing radial position and pressure. See Figs. 13–15. The effect of inertial forces is therefore primarily of importance in the close vicinity of the wellbore. Compared to the capillary and the gravitational force, in particular, the inertial force is relatively more important as pressure is reduced. Since the crookedness of the porous medium is reciprocal to the pore velocity, as presented in Eq. (24), the

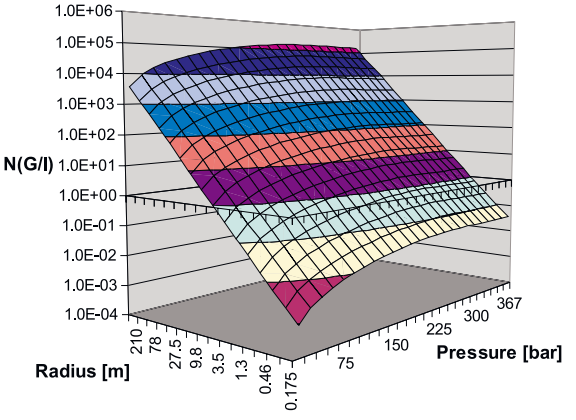

Fig. 15. Normalized ratio of inertial and gravitational forces.

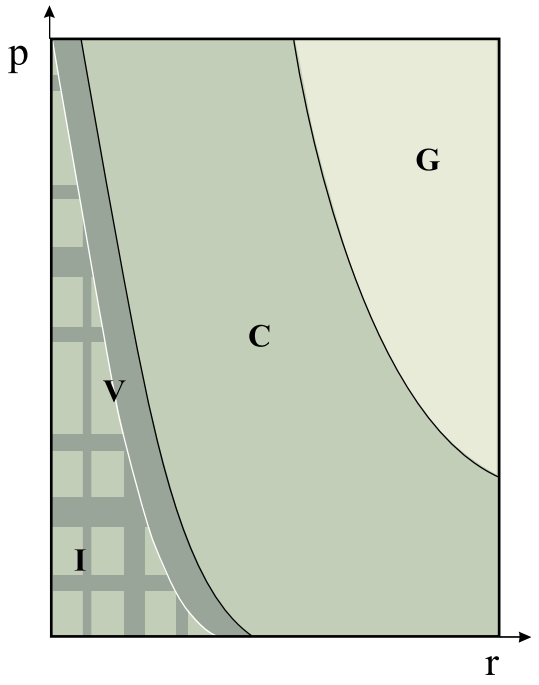

Fig. 16. Representation of forces and their region of importance relative to radial dimension and reservoir pressure.

inertial force may be relatively more important in those parts of the reservoir. Gravitational segregation is therefore less likely in those parts of a reservoir where the effective crookedness is large. In the bulk part of the reservoir, it is safe to neglect the effect of the inertial force, as the fluid flow here is primarily defined by the viscous, the capillary and the gravitational force.

2. The viscous force is proportional to the pore velocity and thus relatively more important than both the capillary and the gravitational force close to the wellbore. Compared to the capillary force, as seen in Fig. 10, the viscous force is, on the other hand, relatively reduced as the pressure is reduced, primarily due to the increase in interfacial tension as function of pressure. In the bulk part of the reservoir where an increased capillary forced is experienced, a stiffening of the interfacial boundaries between gas and liquid condensate may increase the general dynamic pressure drop.
3. The ratio of viscous to gravitational force, as seen in Fig. 11, shows that the likelihood of condensate segregation is greatest in the remote area of the reservoir, furthest away from the wellbore. As generally pore velocity and condensate viscosity are increasing as pressure is decreasing, the importance of condensate segregation, if present at all, is more pronounced at early times of liquid–gas condensation, and at a relatively high average reservoir pressure.
4. In the comparison between the capillary and the gravitational force, see Fig. 12, the increase observed is mainly due to the increase in interfacial tension, slightly dampened by the effect of marginally increasing density difference between condensate and gas.

Fig. 16 is an illustration of some of the points mentioned above. The various forces are characterized by their likelihood of being the dominating force in comparison to the other. The figure gives a very general representation of the ratios of forces as function of radial dimension and reservoir pressure.

4. Effective gas permeability

The formation of liquid condensate will reduce the reservoir effective gas permeability, since the liquid will occupy parts of the volume in the porous media that previously were used for gas flow (Pope et al., 1998). The presence of liquid condensate can reduce the flow of gas through sections of the reservoir or in the worst case totally block the gas transport through certain pores, leading to general rearranging of gas flow patterns in the reservoir (Coskuner, 1997). The presence of liquid condensate will eventually also lead to two-phase flow behavior and reduced gas permeability at condensate saturations higher than the critical condensate saturation S_{cc} (Ali et al., 1997). The definition of S_{cc} is normally associated to a saturation level at which the condensate becomes continuous and starts to flow. In gas condensate reservoirs, this saturation can vary considerably from a few percent up to, i.e., 50%, all depending on the porous medium, wettability strengths and the fluid characteristics.

Fig. 17 shows the condensate saturation defined through a constant volume depletion experiment (CVD), based on the reservoir fluid presented in Table 1. The saturation is given in % and shows a maximum condensate saturation of 3.87% at 135 bar. The actual

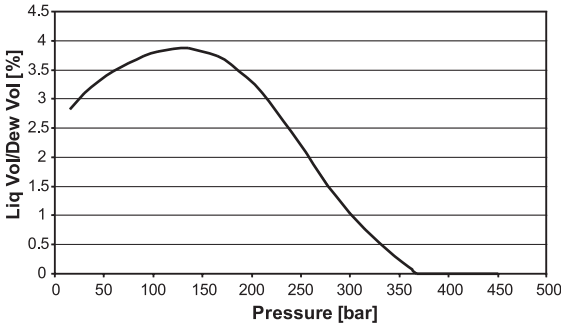

Fig. 17. Condensate saturation in %, defined as part of a constant volume depletion (CVD) experiment, where the the saturation is defined: S_C = Liquid volume/Dew point volume.

condensate saturation in the reservoir $S(r,t)$, on the other hand, is presently not at hand as an analytical model. Even though the maximum condensate saturation is rather low, as in Fig. 17, the cumulative saturation close to the wellbore may eventually become larger than the critical saturation, i.e. $S(r,t)>S_{cc}$. Fig. 18 depicts the cumulative condensate saturation as function of radial dimension. When the saturation exceeds the critical saturation, liquid condensate may flow towards the wellbore, reducing the saturation back to the critical level.

4.1. Space and time relations

In the case of natural gas depletion, the pressure is reduced differently in different parts of the reservoir as time goes on. Similarly is the formation of liquid condensate in the reservoir expected to be a function of both space and time, as mentioned above. Fig. 19 is an illustration of the process of liquid formation as function of fluid phase behavior and radial reservoir pressure. The two-phase region, as shown in the figure, is a cylindrical region progressing radially in to the reservoir.

The formation of condensate may form lenses of liquid, bridging the whole pore volume. Alternatively, the liquid may spread as a thin film over the mineral surface or over the connate water if water is the preferred wetting fluid. The liquid could in other cases reside in the porous medium as monolayers of various extension (Coskuner, 1999).

When the pressure drops below the dew point pressure, the initial formation of liquid condensate is expected to form in those cavities where the local pressure is lowest (Firoozabadi, 1999). The local variation of the pressure in a single pore will depend on the wetting preferences and consequently on the capillary pressure difference. In a porous medium where the liquid condensate is the preferred phase, the first condensation will take place in the narrowest parts of the pore. As the condensation process progresses, the liquid phase is gradually expanding from this point. Finally, droplets of liquid are formed and depending on the relative strength of capillary and gravitational forces, the droplet may start to move freely in the gas or alternatively, in the presence of relative strong gravitational forces, move to the lower side of the mineral grain (Coskuner, 1999).

The formation of liquid condensate in the reservoir happens first in the close vicinity of the wellbore, under the influence of relatively strong viscous forces. The ratios of viscous forces to capillary or gravitationally forces, as depicted in Figs. 10 and 11, show that liquid formed in this part of the reservoir is subjected to strong shear forces and would most probably be immediately transported to the wellbore (Henderson et al., 1996). The effective gas permeability may therefore only be slightly reduced in this part of the reservoir.

In contrast to this situation, when the pressure in the reservoir is reduced to such an extent that the formation of liquid condensate can also take place in the outer part of the reservoir, the ratio of forces will be quite different. At relatively low viscous forces, the ratio of capillary and gravitational forces, as shown in Fig. 12, is characterizing the competition between the forces. Early in the production period, at relatively

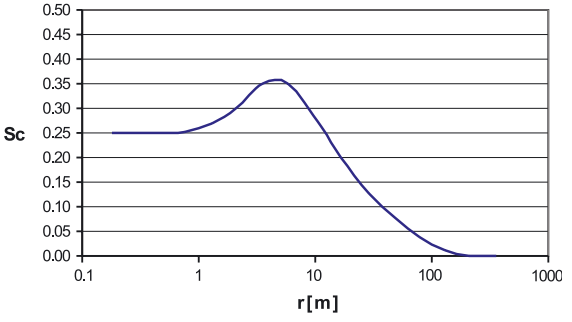

Fig. 18. Cumulative condensate saturation as function of radial dimension.

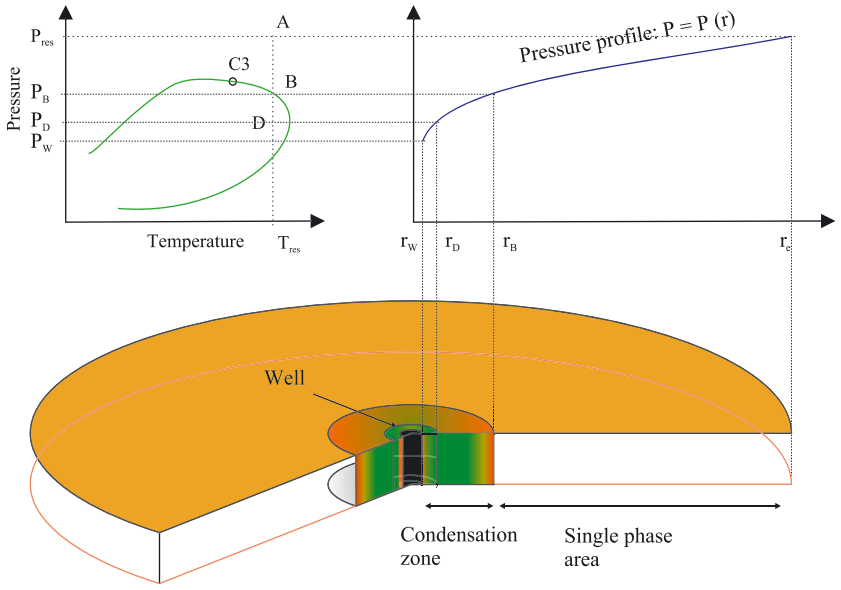

Fig. 19. Formation of liquid condensate related to fluid phase and reservoir pressure draw-down.

high reservoir pressures ($p < p_{dew}$) the gravity force may be dominating. Under these conditions, the liquid may appear as pendant droplets, only partly restricting the porous gas flow. As the pressure is reduced, the relative strength of capillary force is increased, proportional to the increase in the interfacial tension. As a result of this increase, a stiffening of the liquid interface and thus an increased hindrance of gas flow is experienced (Singh et al., 2001). In the absence of viscous forces, but at the same level of condensate saturation, the effective gas permeability would vary depending on the fluid pressure. This observation supports the assumption that the relative gas permeability, traditionally presented as a function of saturation alone, also is dependent on the absolute pressure level, i.e., $k_{rg} = k_{rg}(S_g, p)$.

The amount of liquid condensate present in the porous system, defined by the condensate saturation, is obviously a very important factor in the assessment of effective gas permeability (Bourbiaux, 1994). As the saturation of gas condensate increases above what is commonly known as the critical saturation, two-phase flow will take place in the reservoir and the effective gas permeability is reduced accordingly. In the presence of strong viscous forces, the critical saturation would most likely be lower than in those parts of the reservoir where viscous flow is low. From this, we may conclude that the endpoint relative permeability of liquid condensate will vary with the gas flow rate and thus that the relative gas permeability is rate dependent, i.e., $k_{rg} = k_{rg}(S_g, p, q_g)$.

The dynamical situation of gas flowing towards the wellbore, at decreasing reservoir pressure, will eventually cause the drop out of condensate in all parts of the reservoir (as in this example). The saturation of liquid condensate as seen radially from the outer boundary of the reservoir (r_e) towards the wellbore will be a monotonically increasing function up to a level of the critical condensate saturation where the liquid starts to flow. Closer to the wellbore, the viscous force will reduce the liquid saturation due to increased effect of shear forces (Kalaydjian et al., 1996). See also Fig. 18.

4.2. Reduced gas permeability

The effect of liquid dropout in the reservoir during normal production will undoubtedly lead to reduced gas permeability. The question is how much, where and when?

The general behavior of the reservoir gas permeability in space and time will follow a functional form determined by the local gas saturation, where $k_g(S_g)$ is some increasing function. The point here is not to

discuss the functional dependence of gas saturation, but more to give an interpretation, based on the previous discussion, of the effect of fundamental forces and their representation as dimensionless numbers. In particular, it has been shown that due to viscous forces, there is a rate dependency, which increases the gas permeability near the well more at low absolute pressures than at high pressure. Similarly, the interfacial tension will reduce gas permeability, less near the well than further away, when the absolute pressure decreases.

Based on calculations of dimensionless numbers as seen above and the elaborations presented in the previous section, we may draw a model representing an imaginable picture of how we believe the gas permeability will change in time and space. Fig. 20 represents such a model, where gas permeability is normalized to one in the case of one-phase gas flow, i.e., depicting relative gas permeability.

Early in the production period, when the pressure is above the dew point pressure, no liquid condensation has jet occurred and the relative gas permeability is equal to one in all parts of the reservoir. The first droplets of liquid are observed in the close vicinity of the wellbore, leading to a moderation in gas permeability. Further away from the well, gas permeability is unchanged. Above a certain critical liquid saturation, condensate is produced into the well. As the bottom hole pressure continuously decreases, a radial pressure region, $p < p_{dew}$, expands in to the reservoir and reaches after a relatively short time (in this example) the outer boundary, r_e. After this time liquid condensate is produced in all parts of the reservoir, and the saturation of condensate is increasing towards the wellbore. Gas permeability is reduced as the saturation of liquid condensate is increased.

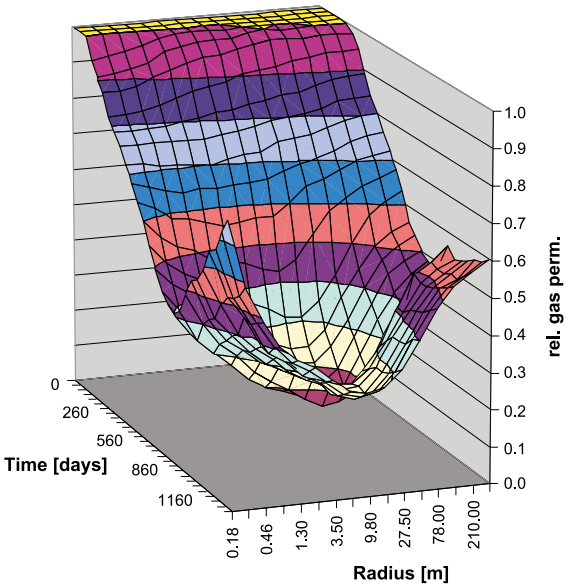

Fig. 20. Relative gas permeability as function of space and time.

This picture will gradually change as the bottom hole pressure is continuously decreased and the viscous forces increases. At this time, the shear forces will become more important and gas saturation close to the well will decrease. The mid-section of the reservoir will experience an increased liquid saturation both due to continued condensation but also due to flow of condensate into the region. These changes in liquid saturation will lead to an increased gas permeability close to the well and a reduced gas permeability in the mid-section of the reservoir. At the outer part of the reservoir, gas permeability is higher than in the mid-section due to low liquid saturation and relatively week viscous forces.

The extended reach of the viscous-dominated region and the fact that liquid condensation will reach an over all maximum per pressure leads to a general increase in gas permeability. This increase is more pronounced close to the wellbore and in the outer part of the reservoir than in the mid-section, where the liquid saturation is the highest.

5. Conclusions

A complete set of dimensionless numbers reflecting the ratios of fundamental forces such as; the capillary, the viscous, the gravitational and the inertial force, has been defined. These numbers are functional dependent on seven independent variables describing fluid, flow and reservoir characteristics.

Based on fluid data from a gas condensate field, applied to a cylindrical test reservoir under somewhat idealized conditions, the various dimensionless numbers have been given a numerical representation. The various numbers constitute a surface spanned by radial dimension and reservoir pressure. The numbers, representing the ratios of fundamental forces, demonstrates a relative dynamical range from 10 to 10^8.

Under the assumption of constant dry gas production, the rather complex process of reservoir fluid behavior, involving liquid dropout in the reservoir and as a consequence, varying gas permeability, has been evaluated in the light of the dimensionless numbers. The relative gas permeability has been estimated, based on the effect dimensionless numbers and the physical conception of increasing condensate saturation in the reservoir. It has been established that the relative gas permeability in the reservoir is not only dependent of the local saturation, but also on flow rate and absolute pressure.

Nomenclature

L	length of cylindrical pore channel
R	radius of cylindrical pore channel
θ	wetting angle
υ_g	pore flow velocity
ΔP_g	pressure drop in gas region
ΔP_o	pressure drop in liquid condensate
ΔP_V	total viscous pressure drop
μ_g	gas viscosity
μ_o	liquid condensate viscosity
P_C	capillary pressure drop
σ_{go}	interfacial tension (gas–liquid)
p	general pressure
p_{dew}	dew point pressure
R_d	spherical droplet radius
g	gravitational constant
Δp_G	gravitational pressure difference
ρ_g	gas density
ρ_o	liquid condensate density
$\Delta\rho_{go}$	density difference
k	absolute permeability
R_r	radius of circular flow path
ΔF_I	Inertial force
A	cross-section of flow path
ΔP_I	inertial pressure difference
ΔL	line segment
$N(C/V)$	ratio of capillary and viscous forces
$N(C/G)$	ratio of capillary and gravitational forces
$N(V/G)$	ratio of viscous and gravitational forces
$N(V/I)$	ratio of viscous and inertial forces
$N(C/I)$	ratio of capillary and inertial forces
$N(G/I)$	ratio of gravity and inertial forces
B_g	gas volume factor
$q_{g,res}$	reservoir volume rate
$q_{g,sc}$	surface volume rate
$\upsilon_{g,bulk}$	reservoir gas flow rate
$\upsilon_{g,pors}$	pore gas rate
r_w	well radius
r_e	well radial boundary
ϕ	reservoir porosity
S_{wc}	connate water saturation
S_g	gas saturation
α	tortuosity angle
Z	gas compressibility factor
T_{res}	reservoir temperature
T_{sc}	surface temperature
R_{MLG}	surface molar liquid gas ratio
S_{cc}	critical condensate saturation
$S(r,t)$	reservoir saturation
k_{rg}	relative gas permeability

References

Ali, J.K., Mcgauley, P.J., Wilson, C.J., 1997. The Effects Of High-Velocity Flow And PVT Changes Near The Wellbore On Condensate Well Performance. Paper SPE 38923 Presented At The 1997 SPE Annual Technical Conference And Exhibition Held In San Antonio, Texas, pp. 5–8. October.

Bourbiaux, B.J., 1994. Parametric study of gas–condensate reservoir behavior during depletion: a study for development planning. Paper SPE 28848 presented at the European Petroleum Conference held in London, UK, pp. 25–27. October.

Coskuner, G., 1997. Microvisual study of multiphase gas condensate flow in porous media. Transport in Porous Media 28, 1–18.

Coskuner, G., 1999. Performance prediction in gas condensate reservoirs. Journal of Canadian Petroleum Technology 38, 8 (August).

Fevang, Ø., Whitson, C.H., Modeling gas-condensate well deliverability, paper 30714, SPE Reservoir Engineering, November 1996.

Firoozabadi, A., 1999. Thermodynamics of Hydrocarbon Reservoirs. McGraw-Hill. Book ISBN 0-07-022071-9.

Fulcher, R.A., Ertekin, T., Sthal, C.D., The effect of the Capullary Number and its constituents on two-phase relative permeability curves, Paper SPE 12170 presented at the 58th Annual Technical Conference and Exhibition held in San Francisco, CA. October 5–8, 1983.

Henderson, G.D., Danesh, A., Tehrani, D.H., Al-Shaidi, S., Peden, J.M., 1996. Measurement and correlation of gas condensate relative permeability by the steady-state method, Paper 31065. SPE Journal. June.

Kalaydjian, F.J.-M., Bourbiaux, B.J., Lombard, J.-M., 1996. Prediction gas–condensate reservoir performance: how flow parameters are altered when approaching production wells. Paper SPE 36715 presented at the 1996 SPE Annual Technical Conference and Exhibition held in Denver, Colorado, USA, pp. 6–9. October.

Morrow, N.R., Songkran, B., 1981. Effect of viscous and buoyancy forces on nonwetting phase trapping in porous media. In: Shan, D.O. (Ed.), Surface Phenomena in Enhanced Oil Recovery, pp. 387–411. In book.

Pedersen, K.S., Fredenslund, Aa., 1987. An improved corresponding states model for the prediction of oil and gas viscosities and thermal conductivity. Chemical Engineering Science 42, 182.

Pedersen, K.S., Fredenslund, Aa., Christensen, P.L., Thomassen, P., 1984. Viscosity of crude oils. Chemical Engineering Science 39, 1011.

Pope, G.A., Wu, W., Narayanaswamy, M., Delshad, M., Sharma, M., Wang, P., 1998. Modeling relative permeability effects in gas-condensate reservoirs. Paper SPE 49266 presented at the 1998 SPE Annual Technical Conference and Exhibition held in New Orleans, Louisiana, pp. 7–30. September.

Raghavan, R., Jones, J.R., Delpletion Performance of Gas-Condensate Reservoirs, Paper SPE 36352, JPT, August 1996.

Singh, M., Mani, V., Honapour, M.M., Mohanty, K.K., 2001. Comparison of viscous and gravity dominated gas–oil relative permeabilities. Journal of Petroleum Science and Engineering 30, 67–81.

Weinaug, C.F., Katz, D.L., 1943. Industrial and Engineering Chemistry 35, 239.

Williams, J.K., Dawe, R.A., Near-Critical Condensate Fluid Behavior in Porous Media—A Modeling Approach, Paper SPE 17137, SPE Reservoir Engineering, May 1989.